International Journal of Nanomedicine

Dovepress
Taylor & Francis Group

Open Access Full Text Article

ORIGINAL RESEARCH

Gold Nanoparticles Functionalized With 5-Amino-2-Mercaptobenzimidazole: A Promising Antimicrobial Strategy Against Carbapenem-Resistant Gram-Negative Bacteria

Jia Zhang[1,2,*], Xiaotuan Zhang[2,3,*], Zhuocheng Yao[2], Juan Pan[2], Jianzhong Ye[2], Ping Xia[2], Tieli Zhou[2], Jianming Cao[1,2]

[1]School of Laboratory Medicine and Life Science, Wenzhou Medical University, Wenzhou, Zhejiang, People's Republic of China; [2]Department of Clinical Laboratory, The First Affiliated Hospital of Wenzhou Medical University, Wenzhou, Zhejiang, People's Republic of China; [3]Department of Clinical Laboratory, The Second Affiliated Hospital, Hengyang Medical School, University of South China, Hengyang, Hunan, People's Republic of China

*These authors contributed equally to this work

Correspondence: Jianming Cao; Tieli Zhou, Department of Clinical Laboratory, The First Affiliated Hospital of Wenzhou Medical University, Key Laboratory of Clinical Laboratory Diagnosis and Translational Research of Zhejiang Province, Wenzhou, Zhejiang, People's Republic of China, Tel +86-577-8806-9595; +86-577-8668-9885, Fax +86-577-8806-9595; +86-577-8668-9885, Email wzcjming@163.com; wyztli@163.com

Introduction: Carbapenem-resistant gram-negative bacteria (CR-GNB) pose a significant threat to public health and require immediate attention. The development of novel antibacterial agents against CR-GNB has become an urgent priority, and nanomaterials offer promising solutions due to their unique properties. This study introduces 5-amino-2-mercaptobenzimidazole (5-A-2MBI) functionalized gold nanoparticles (5-A-2MBI_Au NPs) and evaluates their antibacterial activity against CR-GNB.

Methods: The 5-A-2MBI_Au NPs was synthesized using a one-pot method. Its biocompatibility, bactericidal properties, and mechanisms of action were systematically characterized through in vivo and in vitro toxicity tests, antimicrobial susceptibility testing, live/dead staining, membrane permeability and reactive oxygen species (ROS) generation assays, as well as transcriptomic analysis.

Results: The results of this study demonstrate that 5-A-2MBI_Au NPs exhibit excellent antibacterial efficacy against carbapenem-resistant gram-negative bacteria with various resistance mechanisms, with a minimum inhibitory concentration (MIC) of 2 μg/mL. In vivo experiments further confirmed that 5-A-2MBI_Au NPs not only possess effective bactericidal activity but also exhibit satisfactory biocompatibility. Mechanistic studies revealed that 5-A-2MBI_Au NPs enhance bacterial membrane permeability, increase the generation of reactive oxygen species, and disrupt intracellular oxidative stress and succinate synthesis, thereby conferring potent antibacterial activity. This study results demonstrate that 5-A-2MBI_Au NPs exhibit notable antibacterial efficacy against CR-GNB, with a minimum inhibitory concentration of 2 μg/mL. The antibacterial mechanism involves enhanced membrane permeability, increased reactive oxygen species production, and interference with intracellular oxidative stress and succinate synthesis. These mechanisms collectively contribute to the potent antibacterial activity of 5-A-2MBI_Au NPs against CR-GNB.

Discussion: 5-A-2MBI_Au NPs are a novel and highly effective antibacterial agent prepared through a simple process using benzimidazole and $HAuCl_4 \cdot 3H_2O$. They efficiently eradicate the most challenging multidrug-resistant GNB both in vitro and in vivo while demonstrating excellent biocompatibility. This highlights their potential as a promising antibacterial agent to combat multidrug-resistant GNB.

Keywords: carbapenem-resistant gram-negative bacteria, benzimidazole, gold nanoparticles, biocompatibility, transcriptome analysis

Introduction

As global public health challenges become increasingly severe, antibiotic resistance has emerged as a major concern within the medical community. Traditional antibiotics have long been the cornerstone of bacterial infection treatment, but

Received: 22 October 2024
Accepted: 30 January 2025
Published: 27 February 2025

Graphical Abstract

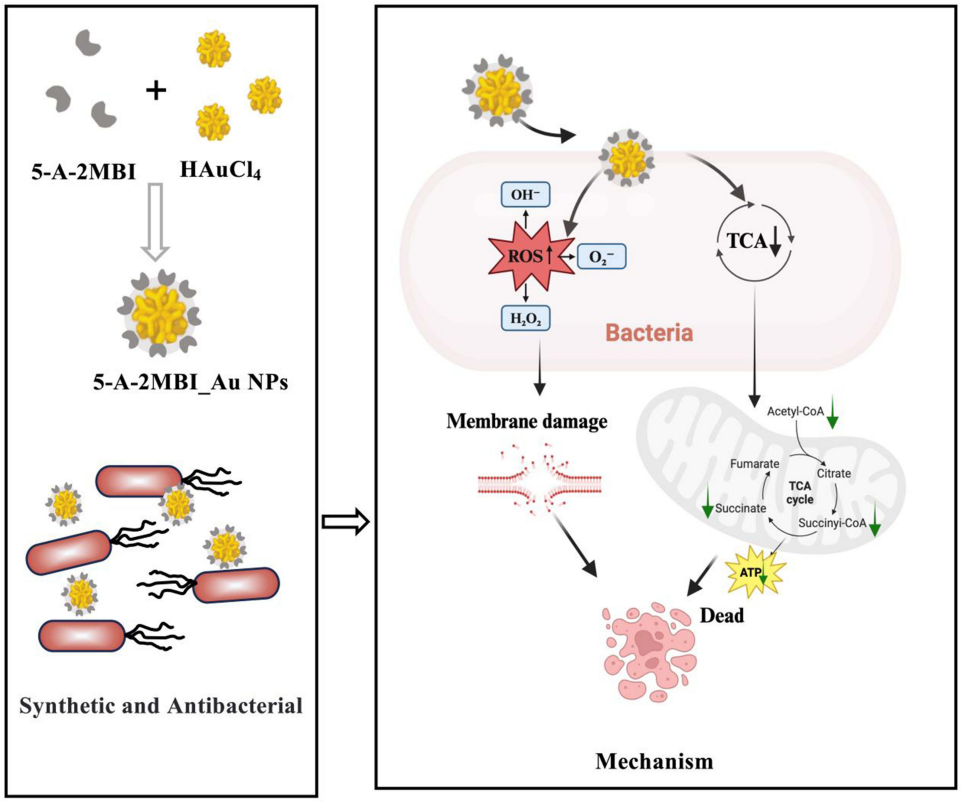

their overuse has led to a rise in resistant strains, especially carbapenem-resistant gram-negative bacteria (CR-GNB).[1,2] CR-GNB exhibits high mortality rates and limited treatment options, making novel antimicrobial agents urgently necessary to combat resistant infections. CR-GNB develops resistance to existing antibiotics and can transfer resistance genes, further complicating treatment options. This phenomenon poses serious threats not only to individual patients but also to public health systems. Consequently, there is an increasing focus on developing antimicrobial drugs with unique mechanisms of action to effectively target these formidable pathogens.[3,4]

Biomedical nanomaterials hold potential for research in a variety of biomedical applications due to their adjustable biocompatibility and ability to reduce toxicity through precise design. Recent advancements in nanotechnology have led to the application of gold nanoparticles (Au NPs) in antibacterial treatment. The unique properties of Au NPs have been utilized in many advanced biomedical applications, such as in vitro and in vivo bioimaging, targeted drug delivery, photoinduction therapy, and cancer treatment.[5] Nanoparticles exhibit diverse antibacterial effects, including reactive oxygen species (ROS) generation, membrane disruption, and metabolic interference. These properties position nanomaterials as crucial tools in the fight against multidrug-resistant infections, and, notably, there have been no reported cases of bacterial resistance to metallic nanoparticles, providing confidence in their clinical applicability.[6–10]

In the field of medicinal chemistry, benzimidazole is a potent pharmacophore with a specific structure-activity relationship (SAR). Benzimidazole and its derivatives have garnered considerable attention for their diverse biological activities, including anti-diabetic, anti-ulcer, and antibacterial properties.[11,12] However, traditional synthesis methods for these compounds are often complex and costly, which limits their broader clinical application. 5-Amino-2-mercapto-benzimidazole (5-A-2MBI) is a precursor for ilaprazole synthesis. Containing both a benzimidazole ring and a mercapto group, 5-A-2MBI possesses strong reducing properties. In this study, we use a simple, rapid, and cost-effective one-pot method for the synthesis of gold nanoparticles (Au NPs).[13] This method leverages the thiol (-SH) group in the 5-A-2MBI

molecule, which interacts with gold ions to form a stable covalent Au-S bond during the reduction process, facilitating the synthesis of 5-A-2MBI-modified gold nanoparticles (5-A-2MBI_Au NPs). We further assessed the antimicrobial efficacy of the synthesized nanoparticles, revealing that 5-A-2MBI_Au NPs demonstrate significant antibacterial activity.

This study investigates the antibacterial effects of 5-A-2MBI_Au NPs against CR-GNB and delves into the underlying mechanisms of action. We hope this study's findings will offer new insights and potential strategies for combating drug-resistant bacterial infections.

Materials and Methods

Isolation of Bacteria and Testing for Antimicrobial Resistance

At the First Affiliated Hospital of Wenzhou Medical University in Wenzhou, China, strains of gram-negative bacteria resistant to carbapenems were identified (Table S1). The strains were detected using MALDI-TOF mass spectrometry (bioMérieux, Lyon, France), which employs matrix-assisted laser desorption/ionization and time-of-flight analysis. Every strain was preserved in a broth with 30% glycerol at −80°C. The strains were revived on blood agar plates (BAPs) and cultured in Luria–Bertani (LB) broth.

The minimum inhibitory concentrations (MIC) of commonly used antibiotics,[14] including imipenem (IPM) and meropenem (MEM), against bacterial strains were determined via the broth microdilution method. The MIC results for the IPM and MEM were interpreted according to the Clinical and Laboratory Standards Institute (CLSI) guidelines. The MICs of the Au NPs, 5-A-2MBI, and 5-A-2MBI_Au NPs were determined separately. Each experiment was conducted three times.

Preparation and Characterization of 5-A-2MBI_Au NPs

We created 5-A-2MBI_Au NPs using a single-step process that included reducing $HAuCl_4 \cdot 3H_2O$, and the synthesis of all the 5-A-2MBI_Au NPs adhered to the described method with minor modifications.[15] First, we added triethylamine (50 μL) and Tween 80 (30 mg) to 10 mL of water and stirred magnetically at 1000 rpm for 20 min at room temperature. $HAuCl_4 \cdot 3H_2O$ (0.05 mM, 40 μL) was slowly added drop by drop to the above mixture (2 mL), followed by 5-A-2MBI (0.05 mM,160 μL), and the mixture was stirred for 1h. The 5-A-2MBI_Au NPs shapes were examined using transmission electron microscopy (TEM, FEI Talos F200S G2, FEI Company, USA) equipped with a field emission electron gun and operated at an accelerating voltage of 200 kV. The charge and dispersion of nanoparticles were evaluated using a nanoparticle size and Zeta-potential analyzer (DLS, Malvern Zetasizer Nano ZS90, UK). For 5-A-2MBI_Au NPs, further structural analysis was conducted using FTIR (Thermo Scientific Nicolet iS20, USA).

Growth Curve

Dynamic monitoring of bacterial growth curves was used to assess the bacteriostatic effect experimentally, following the method previously described.[16] Bacteria in LB medium at a density of 1.5×10^6 CFU/mL were treated with 5-A-2MBI (128 μg/mL), Au NPs (256 μg/mL), and 5-A-2MBI_Au NPs (2 μg/mL) at MIC. The absorbance at OD_{600} was measured with a Multi-Mode Microplate Reader (SpectraMax iD3) for 20 hours.

Time-Kill Assay

Time–kill assays were performed as described previously.[17] The bacteria were subjected to 5-A-2MBI (256 μg/mL), Au NPs (512 μg/mL), and 5-A-2MBI_Au NPs (4 μg/mL), all at a density of 1×10^6 CFU/mL. To serve as the negative control, tubes containing LB alone were used. The bacterial cultures were maintained at 37°C with gentle agitation for intervals of 0, 2, 4, 6, 12, and 24 hours. Serial dilutions by a factor of ten were spread on LB agar plates, and the number of colony-forming units (CFUs) was determined. Each experiment was conducted three times. In a separate set of experiments, the culture medium was supplemented with or without 10mM succinate (Sigma, 224731) in the presence of 5-A-2MBI_Au NPs, and bacterial cultures were incubated under the same conditions at intervals of 0, 2, 4, 6, and 12 hours. CFUs were similarly determined by serial dilution on LB agar plates.

Bacterial Morphology Observation by SEM

Scanning electron microscopy was used to observe the effect of each group on the bacterial cell wall.[18] The bacteria were cultured overnight in LB medium. The starting bacterial density was 1×10^7 CFU/mL. In order to investigate how antibiotics work, we exposed bacteria to 5-A-2MBI_Au NPs (4 μg/mL) on a shaking platform at 37 °C for durations of 2 and 4 hours, maintaining a speed of 200 rpm. Following incubation, the bacteria were preserved using 2.5% glutaraldehyde and then progressively dehydrated with ethanol at different concentrations (30%, 50%, 70%, 80%, 90%, 95%, and 100%) for SEM imaging.

Toxicology Evaluation of 5-A-2MBI_Au NPs

The safety of 5-A-2MBI_Au NPs was assessed using the RBC hemolysis test as previously described.[19] In summary, red blood cells collected from healthy male mice were utilized to prepare a 5% suspension in phosphate-buffered saline. 5-A-2MBI_Au NPs were added to the experimental groups at 1 to 16 μg/mL. Subsequently, the groups were incubated with 5% red blood cells at 37°C for a duration of 2 hours, followed by centrifugation at 3,000 rpm for 5 minutes at 4°C. The absorbance at OD_{450} of the supernatant, which was collected, was measured in a 96-well plate. The PBS group's supernatant acted as the negative control with a 0% hemolysis rate, while the 0.1% Triton X-100 group's supernatant was used as the positive control, showing a 100% hemolysis rate. A hemolysis rate of ≥5% was considered a positive result.

For cell viability assays, 100 μL of HepG2 or HEK-293T cell suspensions containing 5000 cells were seeded into 96-well plates according to the reagent instructions.[20] Subsequently, PBS or different concentrations of 5-A-2MBI_Au NPs was added to the medium and incubated for 24 h. At the end of the incubation period, 10 μL CCK-8 reagent was added to each well and the incubation was continued for 1 h at 37 °C. The absorbance at 450 nm was measured using a microplate reader. The percentage of cell viability was calculated as follows: cell viability (%) = (absorbance of sample -absorbance of medium) / (absorbance of negative control -absorbance of medium) × 100.

To evaluate the toxicity of 5-A-2MBI_Au NPs, SPF male BALB/c mice weighing about 25 g were used. Mice in each group were intraperitoneally injected with 2.5 mg/kg of normal saline as control. Blood was collected after 7 days of continuous intraperitoneal injection, and biological safety was evaluated by detecting serum alanine aminotransferase (ALT), a marker of liver function, and creatinine (Crea), and Urea, marker of renal function.[21] The heart, liver, spleen, lung and kidney of the mice were stained with hematoxylin-eosin and observed under a microscope.

Acute Intra-Abdominal Infection Model

We evaluated the healing impact of 5-A-2MBI_Au NPs through an acute intra-abdominal infection model in mice. To establish an acute peritonitis model, we prepared a bacterial suspension of FK6723 (2×10^7 CFU) in a 5% yeast solution and administered it into the mice's peritoneal cavity. *Klebsiella pneumoniae* FK6723 (bla_{KPC-2}) was randomly selected as a representative strain of CR-GNB for subsequent experiments. After the bacterial challenge, treatments with 5-A-2MBI, Au NPs, or 5-A-2MBI_Au NPs were administered. All the compounds were given via intraperitoneal injection at a dose of 2.5 mg/kg for a total of two doses. As Feng described, the drug delivery scheme for the nitroxoline derivative is based on modification. Twelve hours after infection, 3 mL of sterile PBS was injected into the peritoneum for lavage. The peritoneal lavage fluid (PLF) was then used for colony counting. Regarding ELISA detection, the procedure was executed as previously described with minor adjustments. Kits for detecting IL-1β and TNF-α proteins were utilized following the manufacturer's guidelines.

Animal Care

Four-week-old male ICR mice of SPF grade were sourced from Vital River in Zhejiang, China. Every animal was cared for and housed in a pathogen-free setting at the Laboratory Animal Center of the First Affiliated Hospital of Wenzhou Medical University, provided with sufficient food and water, and kept on a 12-hour light-dark schedule. The mouse experiments were approved by the First Affiliated Hospital Ethics Committee of Wenzhou Medical University (Approval No. SYXK 2021–0017) and carried out in accordance with the Wenzhou Laboratory Animal Welfare and Ethics Guidelines. All experimental mice were euthanized with an overdose of anesthesia.

NPN and PI Membrane Permeability Assays

The permeability of the outer membrane of 5-A-2MBI, Au NPs, and 5-A-2MBI_Au NPs against bacteria was assessed using the probe N-phenyl-1-naphthylamine (NPN) (Aladdin, Shanghai, China) as outlined in a previous study.[22] Following an overnight culture in LB broth, the bacterial strains were rinsed thrice and subsequently diluted with saline solution to achieve an optical density (OD) between 0.3 and 0.4. After exposing the different strains to 5-A-2MBI, Au NPs, or 5-A-2MBI_Au NPs for two hours, the cells were stained with 30 μg/mL of NPN at 37°C for half an hour. Subsequently, the fluorescence intensities were recorded using a BioTek Synergy microplate reader (excitation at 350 nm and emission at 420 nm).

The permeability of the inner membrane was measured using the PI probe. A modified version of the previously described method was used.[23] For two hours, the bacteria were treated with 5-A-2MBI, gold nanoparticles, 5-A-2MBI_Au NPs, or PBS. Subsequently, they received a 30-minute treatment with 50 μg/mL PI. The fluorescence intensity was then measured on a microplate reader (excitation 535 nm, emission 615 nm).

Assessing Membrane Permeability Using SYTO 9 and PI

The bacteria were treated with 5-A-2MBI, Au NPs, and 5-A-2MBI_Au NPs, with PBS as a control.[16] Following the manufacturer's instructions, the bacteria were cultured at 37°C for 12 hours and subsequently stained with SYTO 9 (0.5 mM) and PI (3.0 mM). The samples were observed under a confocal microscope (Nikon A1R-SIM-STORM, Japan) at excitation wavelengths of 488 and 561 nm and emission wavelengths of 530 nm (green) and 617 nm (red).

ROS Production Assays

To quantify the generation of reactive oxygen species (ROS) in bacteria, we used a commercially available kit (Beyotime, Beijing, China) as per previous research.[24] Individual strains of *Escherichia coli, Klebsiella pneumoniae, Enterobacter cloacae, Acinetobacter baumannii*, and *Pseudomonas aeruginosa* were selected for experimentation.

The cultures were rinsed with PBS three times and then diluted to reach a cell concentration with an OD_{600} between 0.3 and 0.4. Subsequently, the cells were exposed to the fluorescent marker DCFH-DA at a 1:1000 dilution, kept in darkness at 37°C for half an hour, and gently inverted and stirred every 3–5 minutes. The probe and cells' full touch were fully confluent. After two hours of treatment with 5-A-2MBI, Au NPs, and 5-A-2MBI_Au NPs, intracellular ROS production was quantified via the use of 10 μM DCFH-DA. Fluorescence intensity was monitored for 2 hours using a 488 nm excitation wavelength and a 525 nm emission wavelength.

Transcriptome Analysis

TRIzol Reagent (Invitrogen Life Technologies) was utilized for RNA extraction, and the RNA's concentration, quality, and integrity were subsequently evaluated using a NanoDrop spectrophotometer (Thermo Scientific). Three micrograms of RNA served as the input for sample preparation. To create sequencing libraries, mRNA was first isolated from the total RNA using magnetic beads attached to poly-T oligos. Fragmentation was triggered by divalent cations at a higher temperature in Illumina's specialized fragmentation solution. The initial strand of cDNA was generated with random primers and Super Script II, whereas the second strand was created using DNA polymerase I and RNase H. Subsequently, overhangs were transformed into blunt ends via exonuclease and polymerase actions, and enzymes were then eliminated. The 3′ ends of the DNA fragments were adenylated, and Illumina PE adapter oligonucleotides were attached to enable hybridization. The resulting cDNA fragments, ranging between 400 and 500 bp, were purified using the AMPure XP system (Beckman Coulter, Beverly, CA, USA).

DNA pieces with attached adaptor sequences at both termini were specifically amplified using the Illumina PCR Primer Cocktail in a 15-cycle PCR process. The products were cleaned using the AMPure XP system and measured with the Agilent high-sensitivity DNA assay on a Bioanalyzer 2100 device. Subsequently, the sequencing library was processed using a Nova Antibacterial Mechanism Seq 6000 system (Illumina) provided by Shanghai Personal Biotechnology Co.Ltd.

Statistical Analysis

All the statistical analyses were conducted via GraphPad Prism 10 or SPSS 22.0 software. The quantitative data are presented as the means ± SDs. For comparisons involving three or more groups, one-way ANOVA and Tukey's post hoc tests were employed, while an unpaired parametric *t*-test was utilized for analyzing two groups. Kaplan-Meier analysis was employed to evaluate survival rates. The data analysis was conducted with a significance threshold of P less than 0.05.

Results

Characterization of the Synthesized 5-A-2MBI_Au NPs

Dynamic light scattering (DLS) revealed that the average size of the 5-A-2MBI_Au NPs was 16.69 nm, with a polydispersity index (PDI) of 0.256 (Figure 1A). These results indicate that the particles are small and uniformly dispersed. In addition, the zeta potential measurements of the 5-A-2MBI_Au NPs revealed an average value of −25.7 mV, suggesting that the nanoparticles are negatively charged and possess good stability. The successful preparation of 5-A-2MBI_Au NPs was further confirmed by Fourier transform infrared (FTIR) analysis, which revealed characteristic peaks at 2495 cm^{-1}, indicating the presence of S-H bonding (Figure 1B). Transmission electron microscopy (TEM) analysis was performed to characterize the ultra-small structure of the as-prepared 5-A-2MBI_Au NPs, and the particle morphology and aggregation behavior were studied. The TEM images revealed that the 5-A-2MBI_Au NPs exhibited an irregular, quasicircular morphology, excellent dispersion, and a uniform particle size distribution (Figure 1C). As demonstrated in Figure 1C, the lattice fringe spacing observed in the high-resolution TEM image measured 0.23 nm, aligning with the face-centered cubic (fcc) gold lattice structure.[25] TEM mapping revealed S and Au localization on the 5-A-2MBI_Au NPs (Figure 1D), confirming that the gold nanoclusters were coated by 5-A-2MBI.

Antimicrobial Properties of 5-A-2MBI_Au NPs

In this study, we assessed the antimicrobial properties of 5-A-2MBI_Au NPs by determining their minimal inhibitory concentration (MIC) against different CR-GNB strains (Table 1).

A total of 17 strains of CR-GNB were collected, including 4 strains each of *Escherichia coli, Klebsiella pneumoniae*, and *Enterobacter cloacae*; 3 strains of *Acinetobacter baumannii*; and 2 strains of *Pseudomonas aeruginosa*. Whole-genome sequencing has verified that the main defense mechanism of CRE is the generation of Ambler class B β-lactamases, including NDM-5, NDM-7, and IMP. Furthermore, additional resistance mechanisms like OXA-23, OXA-66, OXA-486, and KPC have been identified. The MICs of Au NPs and 5-A-2MBI were 256 μg/mL and 128 μg/mL, respectively. These data indicate that these agents do not possess significant antibacterial activity individually. In contrast, 5-A-2MBI_Au NPs effectively inhibited CR-GNB strains with a 2 μg/mL MIC.

One bacterial strain from different genera was randomly selected for growth curve analysis to further study the antibacterial properties and mechanism of 5-A-2MBI_Au NPs in vitro. We observed the growth dynamics of CR-GNB strains under the condition of the MIC of 5-A-2MBI_Au NPs. During the experiment, bacterial growth was monitored every 10 minutes for a continuous period of 20 hours. Bacteria exposed to 5-A-2MBI and Au NPs presented growth curves similar to those in phosphate buffer (PBS), indicating significant bacterial growth (Figure 2A). However, the 5-A-2MBI_Au NPs group exhibited better antimicrobial effects. Additionally, regarding bactericidal kinetics, 5-A-2MBI_Au NPs (4 μg/mL) demonstrated a strong antibacterial effect in the time-killing assay, reducing bacterial growth by more than 2 $\log_{10}$ CFU/mL within 24 h across all five experimental strains (Figure 2B).

In order to better understand how 5-A-2MBI_Au NPs work, we employed field emission scanning electron microscopy (FE-SEM) to examine changes in cell shape and identify any damage to the cell membrane. In the PBS, 5-A-2MBI, and Au NPs groups, FK6723 cells exhibited smooth, intact cell walls and typical rod-shaped morphologies. In contrast, FK6723 cells treated with 4 μg/mL 5-A-2MBI_Au NPs presented rough bacterial surfaces, significant structural alterations, and membrane damage, including pore formation, after 2 hours of exposure. After the 4-hour period, the FK6723 cells showed significantly increased structural degradation, including extensive cell wall damage and leakage of internal contents (Figure 3).

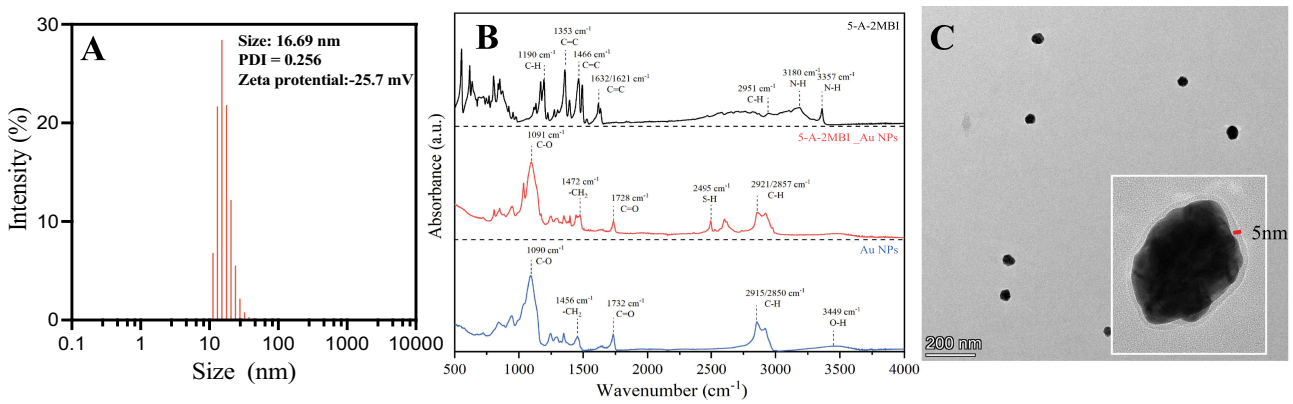

D

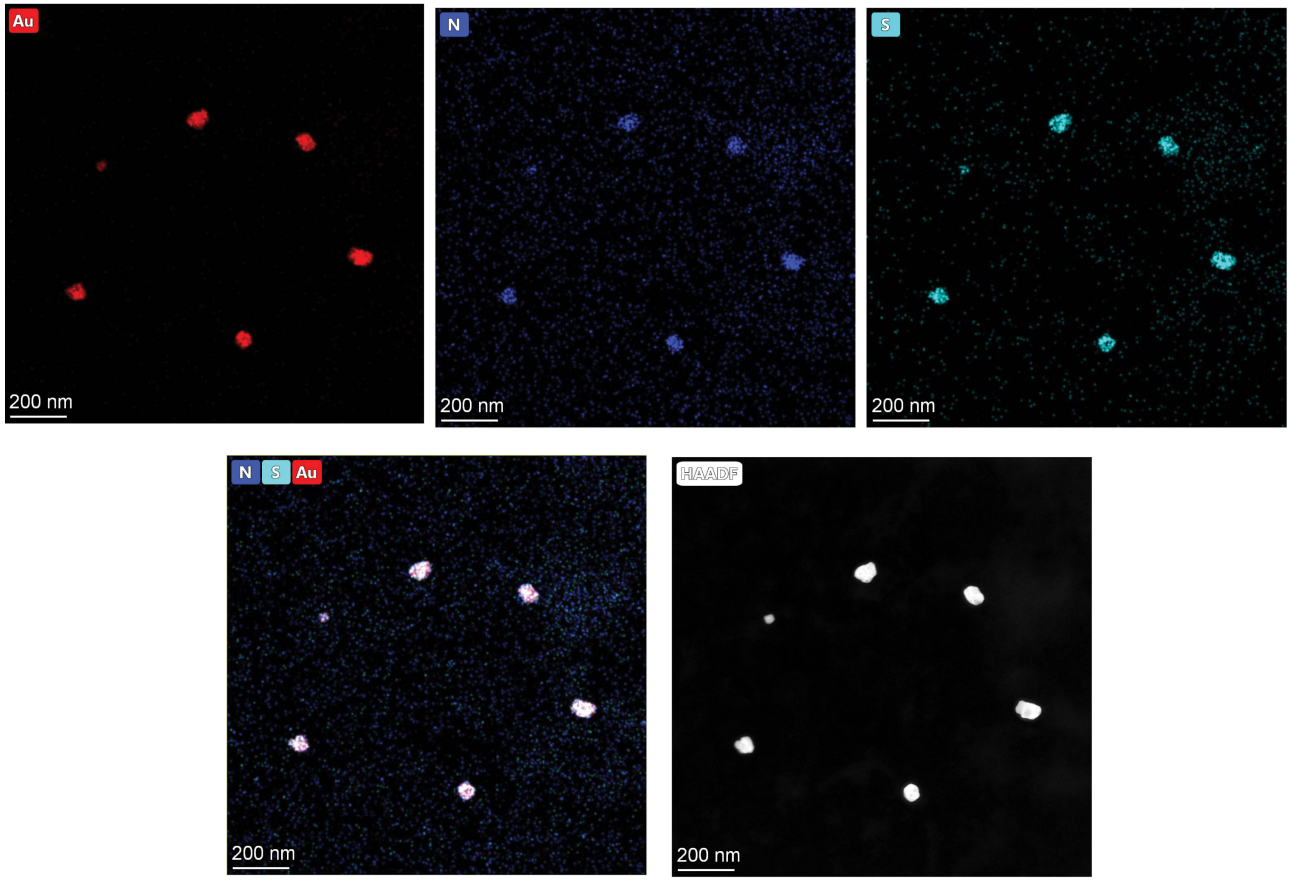

Figure 1 Characterization of 5-A-2MBI_Au NPs. (**A**) DLS analysis of the 5-A-2MBI_Au NPs. (**B**) FTIR spectra of 5-A-2MBI and 5-A-2MBI_Au NPs. Black: 5-A-2MBI; Red: 5-A-2MBI _Au NPs; Blue: Au NPs. (**C**) TEM image of 5-A-2MBI_Au NPs. (**D**) Chemical components and images of 5-A-2MBI_Au NPs analyzed by TEM mapping.

Assessment of Antibacterial Activity in an Animal Model of Acute Intra-Abdominal Infection

The in vivo results demonstrated that 5-A-2MBI_Au NPs significantly enhanced the survival rate of mice with acute intra-abdominal infection (Figure 4A). In cases of acute intra-abdominal infection, 5-A-2MBI_Au NPs decreased the bacterial load in the mice's peritoneal lavage fluid (PLF) (Figure 4B). Moreover, the number of leukocytes in the ascites of the 5-A-2MBI_Au NPs group was lower compared to the other three groups, indicating well-controlled intra-abdominal infection (Figure 4C).

https://doi.org/10.2147/IJN.S502139

Table 1 Antimicrobial Susceptibility of the 5-A-2MBI, Au NPs, and 5-A-2MBI_Au NPs Against Carbapenem-Resistant Gram-Negative Bacteria (CR-GNB) Strains

Species	Strain	Antimicrobial Mechanism	Antimicrobial Susceptibility (MIC, μg/mL)				
			IPM	MEM	5-A-2MBI	Au NPs	5-A-2MBI _Au NPs
E. coli	DC11723	bla_{ndm-5}	32	64	>128	>256	2
	DC10302	bla_{NDM-7}	32	64	>128	>256	2
	DC8439	bla_{NDM-9}	16	64	>128	>256	2
	DC12843	bla_{NDM-9}	16	32	>128	>256	2
K. pneumoniae	FK6719	bla_{KPC-2}	64	256	>128	>256	2
	FK6723	bla_{KPC-2}	64	256	>128	>256	2
	FK9250	bla_{NDM-5}	128	128	>128	>256	2
	FK7079	bla_{IMP-8}	8	4	>128	>256	2
E. cloacae	CG1330	bla_{NDM-1}	8	16	>128	>256	2
	CG1737	bla_{NDM-5}	32	64	>128	>256	2
	CG1591	bla_{IMP}	8	8	>128	>256	2
	CG1640	bla_{kpc-2}	64	64	>128	>256	2
A. baumannii	BM6913	bla_{OXA-23}, bla_{OXA-66}	32	16	>256	>128	2
	BM6927	bla_{OXA-66}, bla_{OXA-23}	32	64	>256	>128	2
	BM6613	bla_{NDM-1}, bla_{OXA-23}, bla_{OXA-66}	256	256	>256	>128	2
P. aeruginosa	TL7559	$bla_{OXA-486}$	32	16	>256	>128	2
	TL8319	bla_{KPC}	32	8	>256	>128	2

In the ELISA tests, kits for detecting IL-1β and TNF-α proteins were used to quantify cytokine concentrations in the blood supernatant of mice following centrifugation. As shown in Figures 4D and E, the concentrations of IL-1β and TNF-α proteins were markedly reduced in the 5-A-2MBI_Au NPs group relative to the PBS group. The decrease in IL-1β and TNF-α indicates successful infection management post-treatment.

Biosafety and Toxicology Evaluation of 5-A-2MBI_Au NPs

The hemocompatibility of 5-A-2MBI_Au NPs was assessed through hemolysis experiments. As shown in Figure 5A, the results indicated that erythrocytes treated with various concentrations of 5-A-2MBI_Au NPs exhibited no hemolytic activity. These results indicate that 5-A-2MBI_Au NPs are suitable for a wide range of safe blood contact applications.

The liver, a crucial organ for processing foreign substances, is frequently exposed to highly reactive or toxic drugs. Such exposure can lead to liver damage characterized by inflammation, oxidative stress, and necrosis.[26] Additionally, any compound is carried to the kidneys in large quantities, significantly increasing the likelihood of toxin exposure.[27] The kidneys are crucial for the processing and elimination of gold nanoparticles. Studies have shown that nanoparticles' size, surface charge, and coating can influence their renal clearance and biodistribution. Smaller nanoparticles are generally cleared more rapidly via the kidneys, reducing potential toxicity. Conversely, bigger nanoparticles often gather in organs like the liver, potentially causing extended retention and negative impacts.[28,29] Therefore, we chose human hepatocellular carcinomas HepG2 cells and human Embryonic Kidney (HEK) 293T cells for cytotoxicity experiments. The results showed that at our experimental concentration, 5-A-2MBI_Au NPs had no cytotoxicity on hepatocytes and kidney cells (Figure 5B and C).

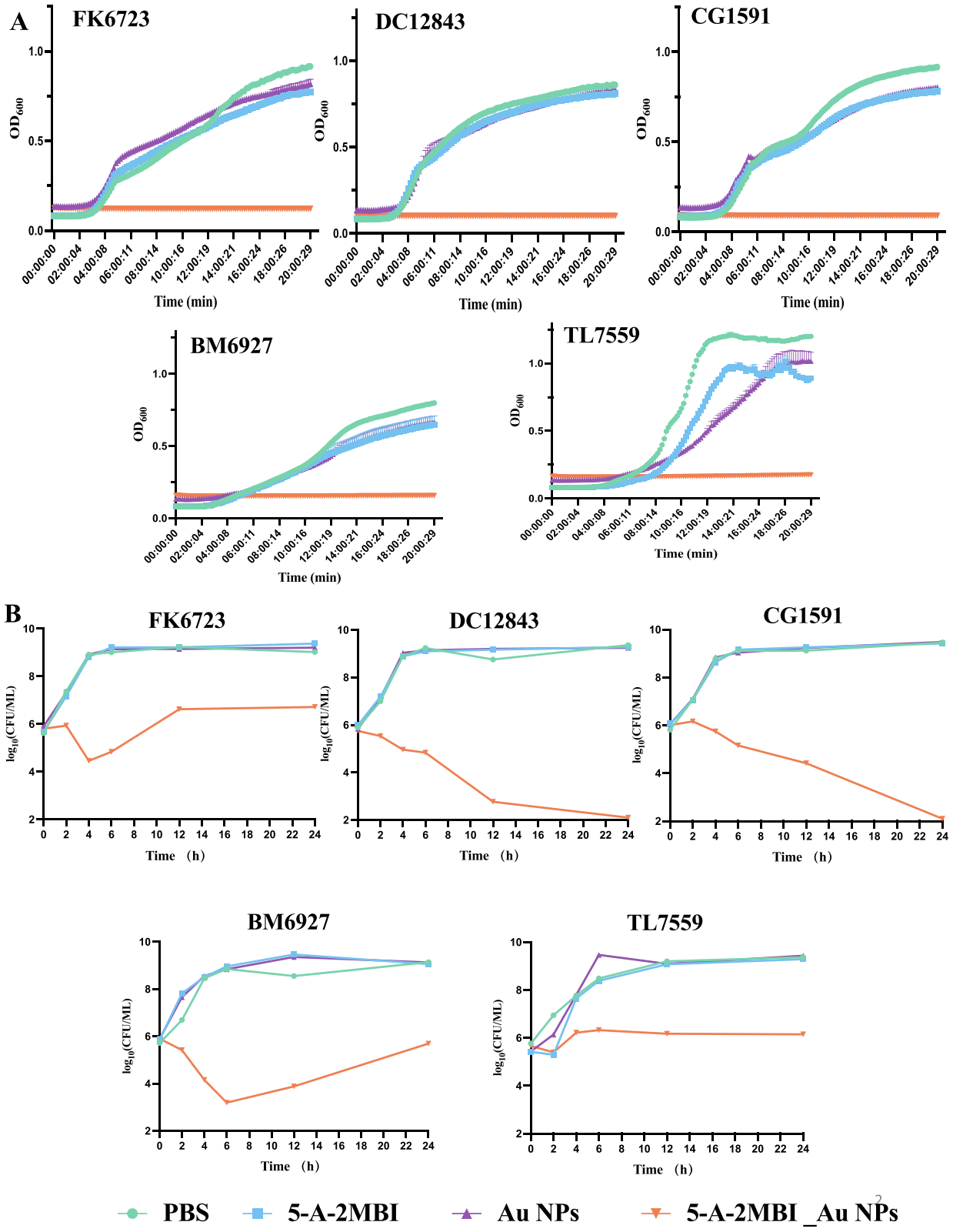

Figure 2 Antimicrobial ability of 5-A-2MBI_Au NPs in vitro. (**A**) Growth curves of clinical CR-GNB strains after treatment with different formulations. (**B**) Time–killing curves of PBS, 5-A-2MBI, Au NPs, or 5-A-2MBI_Au NPs.

https://doi.org/10.2147/IJN.S502139

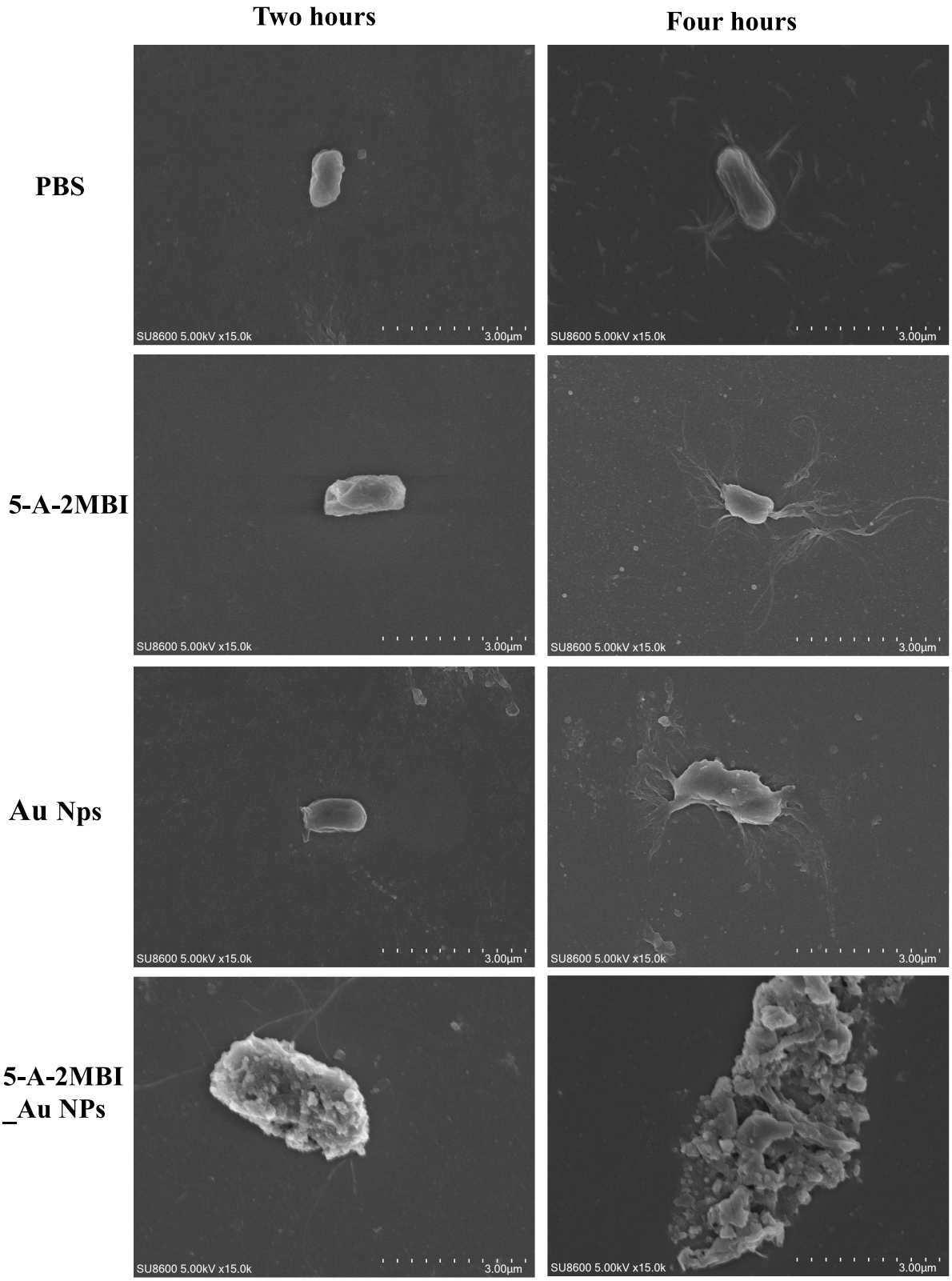

Figure 3 SEM images of FK6723 strains showing bacterial morphology after treatment with different formulations.

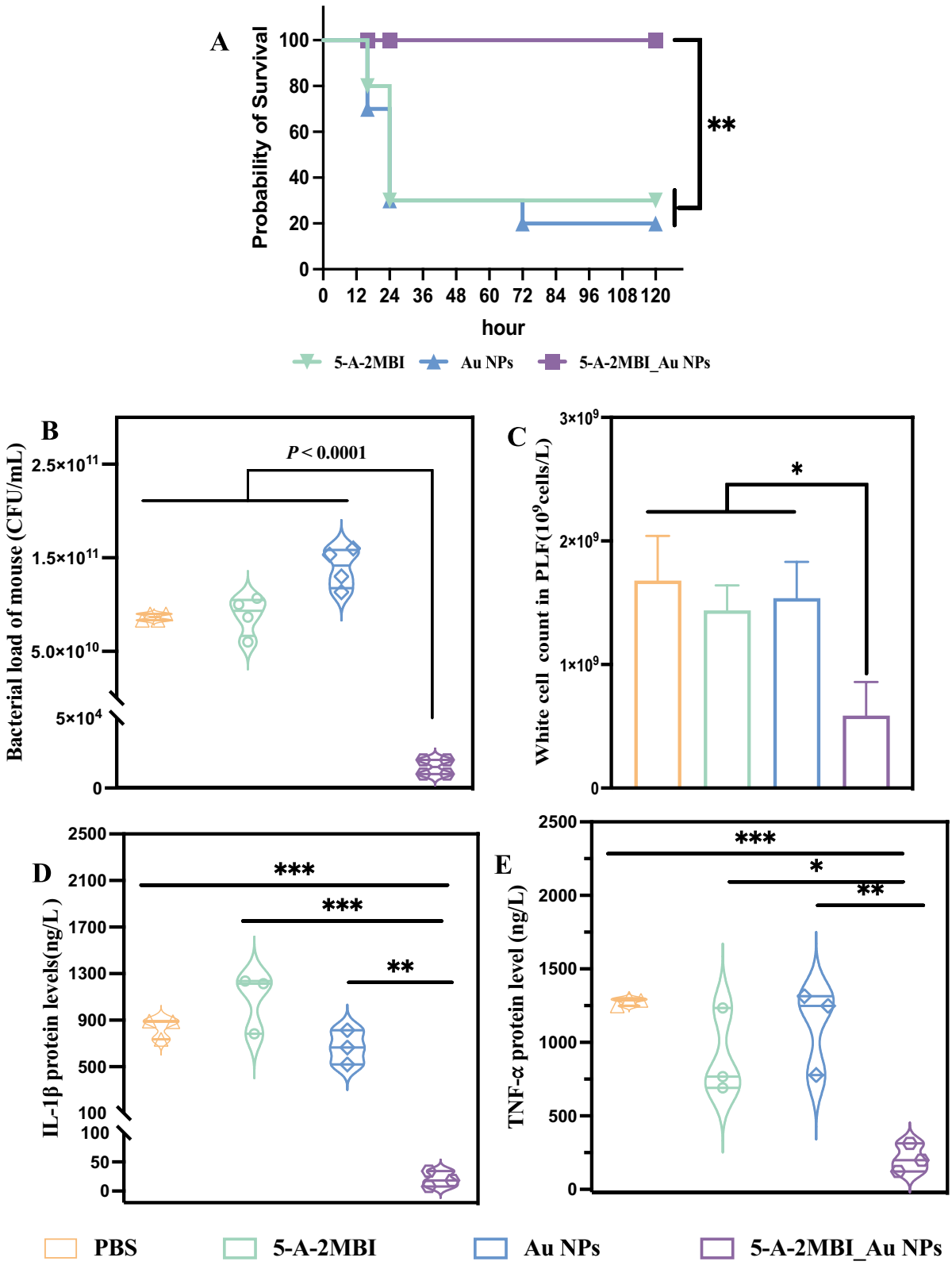

Figure 4 Mouse survival curve and acute intra-abdominal infection model. (**A**) Survival curves of mice infected with 5-A-2MBI, Au NPs, or 5-A-2MBI_Au NPs. (**B**) Quantification of bacteria in the abdomen of mice with FK6723 infection after 12 h of different treatments. (**C**) White blood cell count in the peritoneal fluid of a mouse model of acute peritonitis. (**D** and **E**) ELISA was performed to measure the levels of IL-1β and TNF-α in the blood of the mice. The data were evaluated using one-way ANOVA (*$P < 0.05$; **$P < 0.01$; ***$P < 0.001$).

https://doi.org/10.2147/IJN.S502139

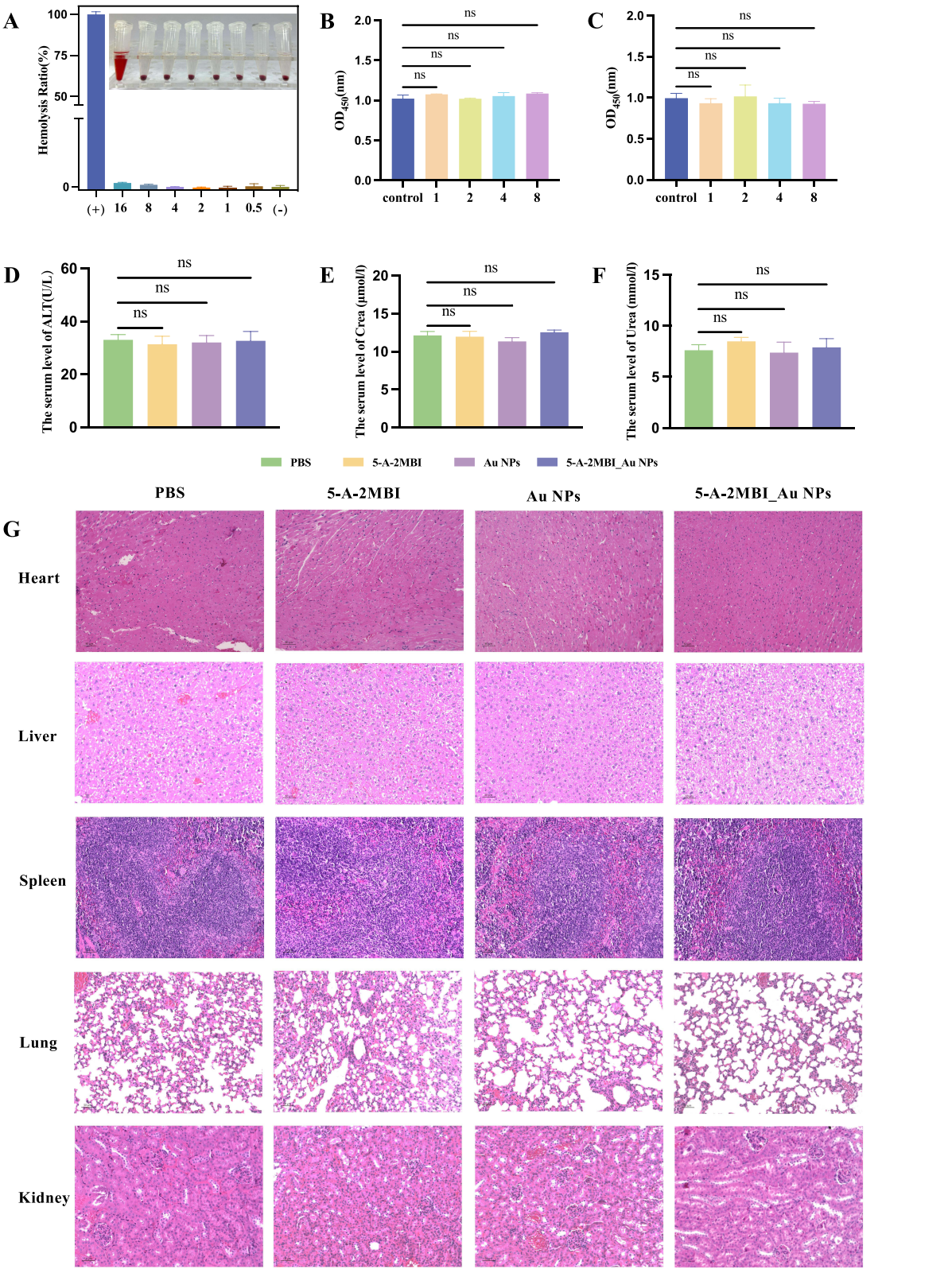

Figure 5 Safety evaluation of the hemolytic effects of 5-A-2MBI_Au NPs at various concentrations. (**A**) Hemolytic effects of 5-A-2MBI_Au NPs at various concentrations. (**B** and **C**) The toxicity of 5-A-2MBI_Au NPs at different concentrations in human hepatocellular carcinomas HepG2 cells (**B**) and human Embryonic Kidney (HEK) 293T cells (**C**) was determined by CCK-8 assay. Statistical differences in OD_{450} readings indicate cytotoxicity. (**D–F**) Serum biochemical biomarkers of alanine aminotransferase (ALT), creatinine (Crea), and urea nitrogen (Urea). (**G**) HE staining was used to observe pathological changes in the organs of the mice on the 7 days after continuous intraperitoneal injection of 5-A-2MBI_Au NPs.

To further understand the biosafety of 5-A-2MBI_Au NPs during treatment, a series of analyses were performed to evaluate the toxicity adverse effects of 5-A-2MBI_Au NPs in mice. Mice were intraperitoneally injected with 5-A-2MBI_Au NPs every 12 hours for 7 days. Serum alanine aminotransferase (ALT), creatinine, and urea levels were not significantly different between the mice and the normal control group on day 7 (Figure 5D–F). 5-A-2MBI_Au NPs do not cause adverse effects on the liver and kidneys. At the same time, the major organs of the mice, including liver, lung, kidney, heart, and spleen, were collected for HE staining, and there were no significant histological damage or inflammatory cell infiltration in these organs (Figure 5G). The above results suggest that 5-A-2MBI_Au NPs have good biocompatibility and provide potential evidence for their safety and potential biomedicine.

Study of Antibacterial Properties and Mechanisms

Gram-negative bacteria possess a slim peptidoglycan layer and an external membrane made up of lipopolysaccharides that are negatively charged. These anionic molecules exhibit a stronger attraction to the cations emitted by the majority of nanoparticles. This results in ion accumulation and heightened absorption, leading to cellular damage.[30] We evaluated the outer membrane's (OM) permeability by employing the fluorescent dye N-phenyl-1-naphthylamine (NPN). Disruption of the OM causes NPN to bind to cell lipids, leading to heightened fluorescence.[31] As shown in Figure 6A, 5-A-2MBI_Au NPs significantly increased OM permeability compared with that of the control and other groups at drug concentrations corresponding to 1/2 MIC and MIC.

We also investigated the effect of 5-A-2MBI_Au NPs on the bacterial inner membrane (IM). To assess the permeability of the cell membrane, we used propidium iodide (PI), a DNA-binding dye (Figure 6B). Consistent with the OM results, 5-A-2MBI_Au NPs significantly increased IM permeability at drug concentrations of 1/2 MIC and MIC.

In addition, we stained bacteria with PI and SYTO 9. PI binds tightly to DNA in cells with compromised membranes, marking them as dead, while SYTO 9 stains all bacterial cells, living or dead.[6] As illustrated in Figure 7A, the bacterial cells in the group treated with PBS displayed intense green fluorescence and lacked red fluorescence when stained with PI, indicating a high number of living bacteria. Similarly, the 5-A-2MBI and Au NPs groups also displayed green fluorescence when stained with SYTO 9, with a slightly weak red fluorescence in the experimental group. However, PI staining revealed red fluorescence in the 5-A-2MBI_Au NPs-treated group. These results indicate that 5-A-2MBI_Au NPs had a significant effect on damaging gram-negative bacteria.

The antibacterial mechanism of gold nanoparticles begins with their penetration, which damages the cell wall. This damage leads to the production of a large amount of ROS.[32] ROS inhibit ATP production and DNA replication. Furthermore, ROS can counter intracellular antioxidant defenses and cause cell wall breakage, further promoting damage to the cell wall. We randomly selected five strains for ROS detection. Under the conditions of 1/2 MIC, the 5-A-2MBI_Au NPs significantly increased the ROS levels (Figure 7B). This finding is consistent with the above hypothesis.

Transcriptome Sequencing Analysis

To better understand the molecular mechanisms by which 5-A-2MBI_Au NPs exert their antibacterial effects, we performed full-transcriptome RNA sequencing to analyze the specific mRNA-level responses. As illustrated in Figure 8A, the FK6723 strain exhibited 55 genes with increased expression and 114 genes with decreased expression when exposed to 5-A-2MBI_Au NPs (|log2 (fold change) | >1, $P < 0.05$).

We performed enrichment analyses using Gene Ontology (GO) and the Kyoto Encyclopedia of Genes and Genomes (KEGG) to pinpoint the metabolic pathways and interactions linked to the antibacterial properties of 5-A-2MBI_ Au NPs. Differentially expressed genes (DEGs) annotated by GO enrichment analysis were significantly involved in various metabolic pathways, such as the one-carbon pool enriched with folate, glycerophospholipid metabolism, phenylalanine metabolism, histidine metabolism, and tyrosine metabolism (Figure 8B). The DEGs were divided into three primary Gene Ontology (GO) categories: biological processes (BP), cellular components (CC), and molecular functions (MF), which included 35, 6, and 20 subcategories, respectively. Within the BP category, the DEGs were mainly associated with ion transmembrane movement, alditol phosphate metabolism, and general transmembrane transport. Within the CC classification, differentially expressed genes (DEGs) were linked to the cell membrane, outer cell boundary, periplasmic

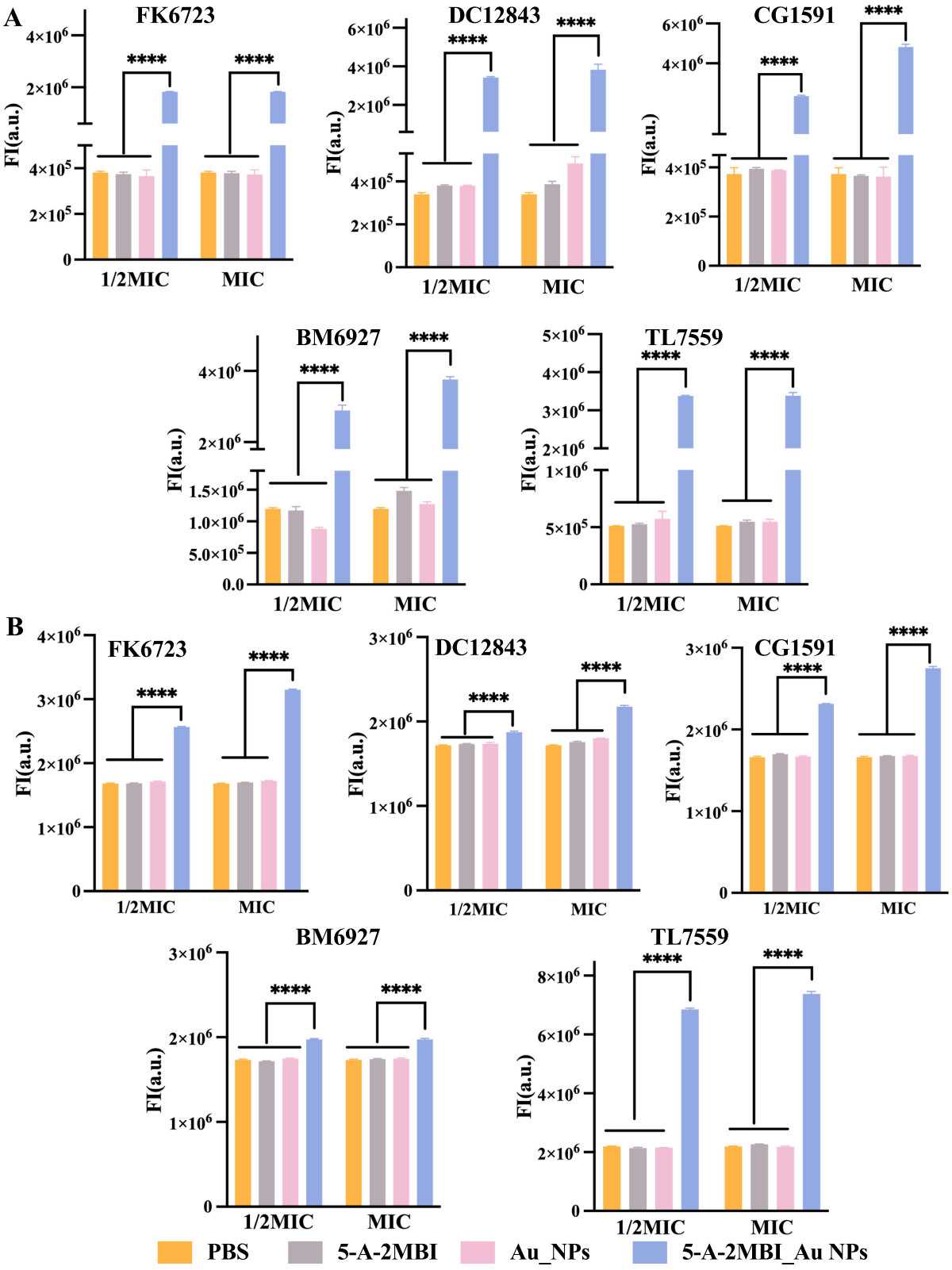

Figure 6 5-A-2MBI_Au NPs inhibit bacterial growth by increasing membrane permeability. (**A**) Fluorescence intensity of NPN after treatment with different treatments. (**B**) Fluorescence intensity of PI after treatment for different treatments. The data were evaluated using one-way ANOVA (****$P < 0.0001$).

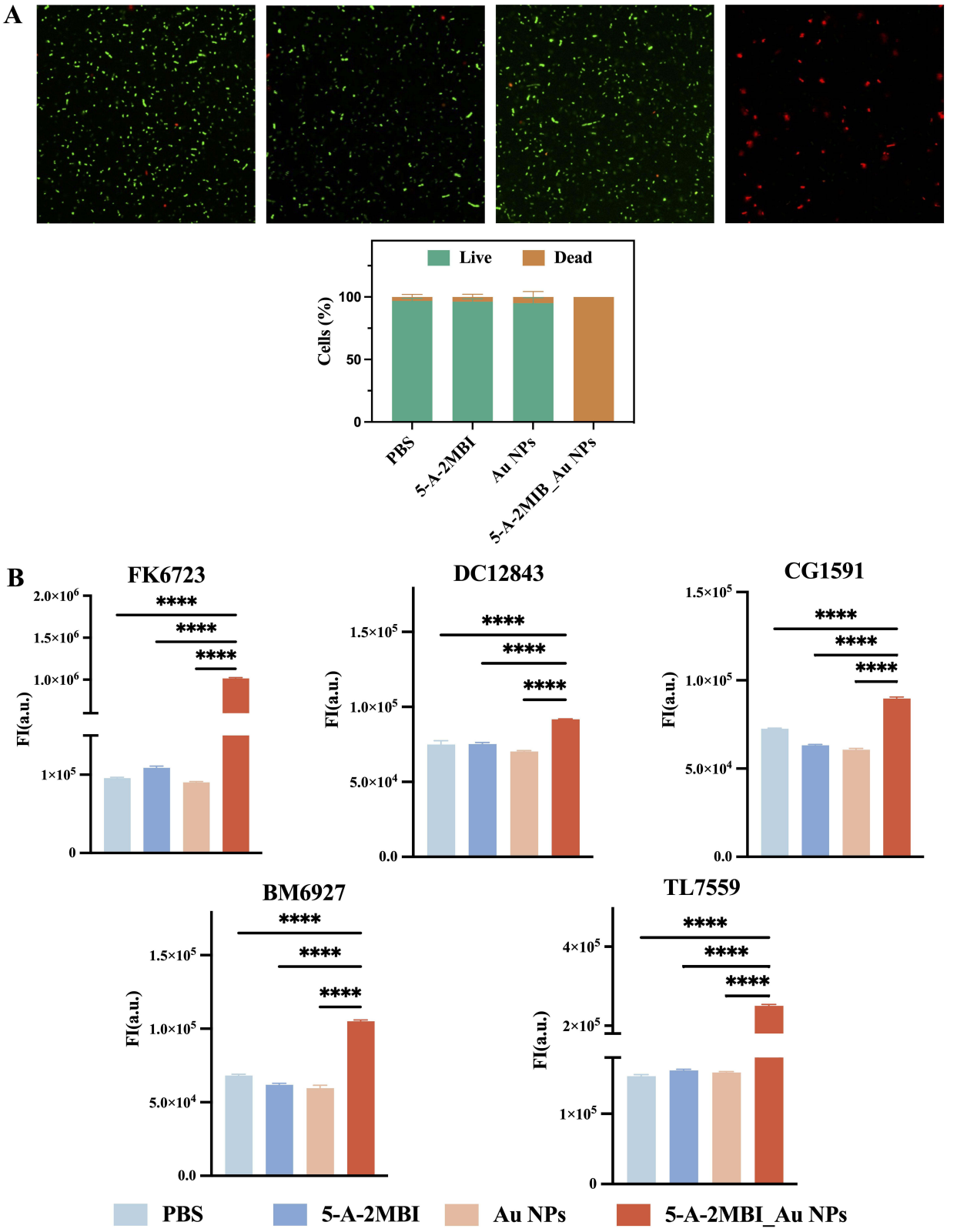

Figure 7 Live/dead staining using SYTO 9 and PI and ROS production. (**A**) Live/dead staining of FK6723 cultured overnight to 0.5 McFarland standard and subjected to different treatments. (**B**) Fluorescence intensity analysis of intracellular ROS in CR-GNB strains using a ROS assay kit after various treatments. The data were evaluated using one-way ANOVA (****$P < 0.0001$).

https://doi.org/10.2147/IJN.S502139

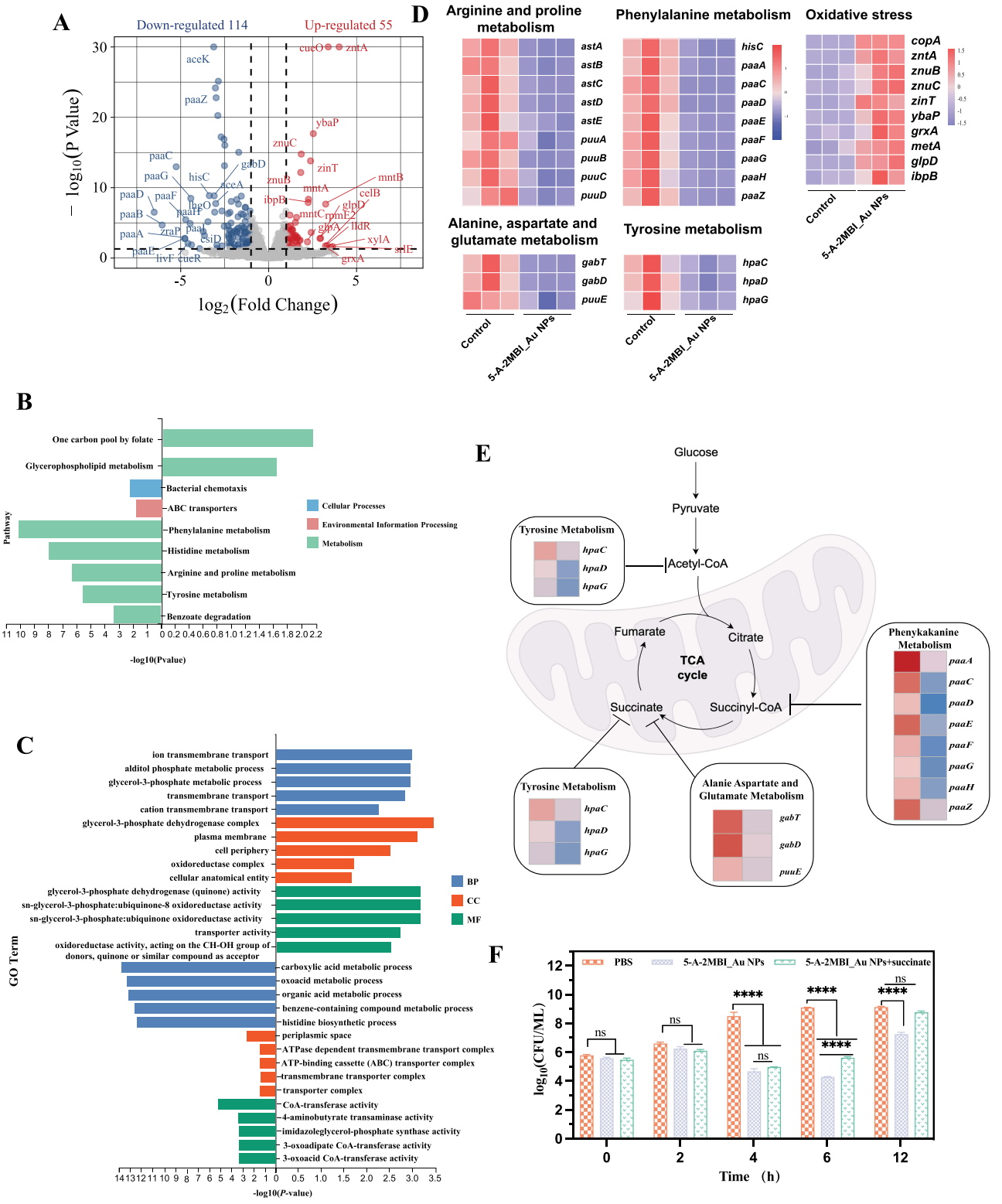

Figure 8 Distribution of DEGs in the 5-A-2MBI_Au NPs treated FK6723 strains. (**A**) Visualization of volcano plots of DEGs. Each dot represents a gene; red dots (significantly up-regulated genes), blue dots (significantly down-regulated genes) and black dots (non-significantly different genes) for each group are indicated on the diagram. (**B**) KEGG enrichment analysis of DEGs. Right: up, Left: down. (**C**) GO analysis of DEGs between the 5-A-2MBI_Au NPs treated and the control groups. Right: up, Left: down. (**D**) Heatmap showing all DEGs. Colors demonstrate expression level patterns in 5-A-2MBI_Au NPs-treated and control groups. The red cluster represents up-regulated expression, and the blue cluster represents down-regulated expression. (**E**) Expression patterns of genes involved in the TCA cycle pathway. (**F**) 5-A-2MBI_Au NPs affect succinic acid synthesis. The PBS group (negative control group; Orange), 5-A-2MBI_Au NPs group (control group, blue), and 5-A-2MBI_Au NPs with 10 mM succinic acid (experimental group, green) were added, indicating metabolites. Survival was measured as colony-forming units (CFUs). The data were evaluated using one-way ANOVA (****$P < 0.0001$).

region, and the ATP-binding cassette (ABC) transporter complex. In the MF category, most DEGs were related to catalytic activity (Figure 8C).

Energy metabolism is crucial for various biological processes, including the growth and survival of organisms. The TCA cycle is crucial for generating energy in the majority of living beings. As shown in Figures 8D and 8E, the TCA cycle in FK6723 cells was significantly affected by 5-A-2MBI_Au NPs treatment. We observed decreased gene expression related to multiple succinate synthesis pathways within the TCA cycle. This reduction in gene expression suggests that 5-A-2MBI_Au NPs disrupt the TCA cycle, thereby impairing bacterial energy metabolism.

To explore the impact of succinate on the TCA cycle when treated with 5-A-2MBI_Au NPs, we added succinate to the medium and observed bacterial growth. We found that bacterial growth increased significantly after 6 hours of incubation with succinate under 5-A-2MBI_Au NPs treatment ($p < 0.05$). These findings indicate that adding succinate partially mitigates the inhibitory effects of 5-A-2MBI_Au NPs on the TCA cycle. Meantime, at 12 hours, the bacterial count in the succinate group was not significantly different from that in the PBS group (Figure 8F).

Discussion

The increasing danger of carbapenem-resistant gram-negative bacteria (CR-GNB) is a global issue. This has significant implications for public health, clinical care, and economic costs. Treating infections caused by these bacteria is difficult due to their high rates of antibiotic resistance, leading to high mortality rates. Consequently, controlling these infections becomes extremely challenging.[33] In Ecuador, a study found that 86.66% of *Klebsiella pneumoniae* bacteria carry KPC genes, making traditional antibiotic treatments ineffective. Patients infected with these antibiotic-resistant bacteria have high morbidity and mortality rates of 17.9%, indicating severe clinical consequences.[34] The resistance mechanisms of CR-GNB are complex and diverse and involve enzymes that hydrolyze carbapenem antibiotics, leading to antibiotic resistance. Fortunately, gold nanoparticles have promising clinical applications, particularly in treating infections caused by antibiotic-resistant strains. The multiple antimicrobial mechanisms and good biocompatibility of gold nanoparticles make it a promising new antimicrobial agent.

For our study, we selected gram-negative bacteria that produce different carbapenemases, such as KPC, NDM, and OXA-48. Surprisingly, we discovered that 5-A-2MBI_Au NPs exhibited outstanding antimicrobial activity at relatively low concentrations. The shape of nanoparticles is crucial for their effectiveness against bacterial cells. In one study, researchers examined the effect of nanoparticle shape on internalization.[35] They reported that spherical particles, which are similar in size, take up 500% more particles than rod-shaped particles do and are less toxic to host cells. To enhance the ability of nanoparticles to enter host cells, we synthesized them to be spherical or nearly spherical, with a compound modification layer of approximately 5 nm thickness on the 5-A-2MBI_Au NPs surface. We conducted hemolysis assays, HE staining of mouse organs, and blood, liver, and renal function tests to ensure safety and biocompatibility. We found that 5-A-2MBI_Au NPs had better safety and biocompatibility. Furthermore, in acute intra-abdominal infection, our findings suggest that 5-A-2MBI_Au NPs have potential anti-inflammatory and bactericidal effects. The reduction in IL-1β and TNF-α suggests effective infection control after treatment.

Owing to their various antimicrobial mechanisms, gold nanoparticles offer unique advantages, including disruption of bacterial cell membranes, induction of oxidative stress, and interference with bacterial metabolic pathways.[8] They can directly interact with the cell wall and membrane of bacteria, leading to disruption of the membrane structure and leakage of cell contents. Bacterial cell membranes are negatively charged, and the interaction with negatively charged Au NPs is likely mediated by mechanisms other than electrostatic attraction, such as ROS generation or physical disruption of the membrane structure. NPN, PI, and SEM experiments fully demonstrated the ability of 5-A-2MBI_Au NPs to significantly disrupt the bacterial cell wall and achieve a bactericidal effect.

Upon entering a bacterial cell, Au NPs disrupts the electron transport chain, causing a notable rise in intracellular reactive oxygen species (ROS). Reactive oxygen species like superoxide anions, hydrogen peroxide, and hydroxyl radicals initiate an oxidative stress response, potentially harming bacterial DNA, proteins, and lipids. To counteract this stress, bacteria activate oxidative stress response mechanisms and increase the expression of antioxidant enzymes to neutralize ROS and reduce damage to the cell.[32] Moreover, our experimental results demonstrate that 5-A-2MBI Au NPs at 1 μg/mL can increase the level of ROS in experimental strains, as evidenced by the increased expression of oxidative

stress response-related genes. One such gene is *grxA*, which encodes glutathione reductase and is involved in the glutathione redox cycle. The glutathione system serves as a major intracellular antioxidant defense mechanism.[36]

In the transcriptome results, we found that genes encoding genes involved in succinate synthesis associated with succinyl-coenzyme production were significantly down-regulated in the tricarboxylic acid cycle pathway. Furthermore, we observed the effect of adding succinate to the culture medium on the bactericidal effect of FK6723 in the presence of 5-A-2MBI_Au NPs. The findings showed that after 6 hours of incubation, the group with added succinate exhibited significantly more bacterial growth compared to the control group without supplementation. These findings are consistent with previously reported studies, including those published in *Science*,[37] which highlight the critical role of succinate in bacterial metabolism and its impact on the tricarboxylic acid cycle. Simultaneously, the existence of 5-A-2MBI_Au NPs mainly impacts ATP generation by altering succinate formation within the TCA cycle. This disruption in succinate production directly impacts the bacterial energy supply, leading to inhibited growth and reproduction. Succinate is an essential component in various metabolic pathways, and any obstruction in the TCA cycle alters the levels of intermediates, thereby affecting other metabolic processes. Furthermore, proper functioning of the TCA cycle is crucial for maintaining the redox balance of the cell. Blocking this cycle can increase ROS levels inside the cell, resulting in oxidative stress.[38] On the basis of this evidence, we conclude that 5-A-2MBI_Au NPs can disrupt energy metabolism and effectively inhibit bacterial growth.

In summary, our study confirms the potential of 5-A-2MBI_Au NPs as clinical antimicrobial agents. Our experiments focused primarily on revealing the antimicrobial properties of these nanoparticles. We demonstrated the safety of 5-A-2MBI_Au NPs at experimentally safe concentrations by in vivo and in vitro experiments. In the meantime, we believe that a more detailed in vivo safety assessment is necessary. Since gold nanoparticles act on bacteria through multiple mechanisms, such as disrupting the cell wall, generating ROS, and regulating metabolism, it becomes more challenging for bacteria to develop drug resistance. This multi-level antibacterial mechanism makes it difficult for bacteria to resist the bactericidal effect of gold nanoparticles through a single mutation or the expression of drug-resistant genes, thereby effectively extending its lifespan and clinical efficacy.

Conclusion

The synthesized 5-A-2MBI_Au NPs demonstrated potent antibacterial activity, particularly against CR-GNB. Safety evaluation experiments showed that the 5-A-2MBI_Au NPs had no obvious toxicity in both in vitro and in vivo models at an effective antibacterial concentration, suggesting that the 5-A-2MBI_Au NPs have the value of further in-depth research. Mechanistically, 5-A-2MBI_Au NPs induced significant ROS generation, disrupted bacterial cell wall integrity, and transcriptional profiling indicated downregulation of succinate synthesis, a key intermediate in the TCA cycle. These findings underscore the potential of 5-A-2MBI_Au NPs as a novel antibacterial agent for combating multidrug-resistant infections while offering new insights into their antibacterial mechanisms.

Abbreviations

CR-GNB, carbapenem-resistant gram-negative bacteria; Au NPs, Gold nanoparticles; 5-A-2MBI, 5-amino-2-mercapto-benzimidazole; 5-A-2MBI_Au NPs, 5-amino-2-mercaptobenzimidazole-modified gold nanoparticles; $HAuCl_4$, Tetrachloroauric acid; MIC, Minimum inhibitory concentration; LB, Luria Bertani; BAPs, blood agar plates; IPM, Imipenem; MEM, Meropenem; PBS, Phosphate-buffered saline; DLS, Dynamic light scattering; PDIs, Polydispersity indices; TEM, Transmission electron microscopy; SEM Scanning electron microscopy FTIR, Fourier-transform infrared spectroscopy; RBC, Red blood cells; PI, Propidium iodide; NPN, N-phenyl-1-naphthylamine; ROS, Reactive oxygen species; SPF, Specific pathogen-free; H&E, Hematoxylin and eosin; ELISA, Enzyme-linked immunosorbent assay; ALT, Alanine aminotransferase; GO, Gene Ontology; KEGG, Kyoto Encyclopedia of Genes and Genomes; SD, Standard deviation; ANOVA, One-way analysis of variance.

Data Sharing Statement

The data used and analyzed in this study are included in this article and are available from the first author upon reasonable request.

Ethics Approval and Informed Consent

The mouse experiments were approved by the First Affiliated Hospital Ethics Committee of Wenzhou Medical University (Approval No. SYXK 2021–0017) and carried out in accordance with the Wenzhou Laboratory Animal Welfare and Ethics Guidelines.

Acknowledgments

This study was funded by Key Laboratory of Clinical Laboratory Diagnosis and Translational Research of Zhejiang Province (2022E10022). We deeply appreciate the support and guidance from JC and TZ during the project. We are also grateful for the collaborative atmosphere and academic assistance within our laboratory community. We thank Scientific Research Center of Wenzhou Medical University for consultation and instrument availability that supported this work.

Author Contributions

All authors made a significant contribution to the work reported, whether that is in the conception, study design, execution, acquisition of data, analysis, and interpretation, or all these areas; took part in drafting, revising, or critically reviewing the article; gave final approval of the version to be published; have agreed on the journal to which the article has been submitted; and agree to be accountable for all aspects of the work.

Funding

This work was funded by Key Laboratory of Clinical Laboratory Diagnosis and Translational Research of Zhejiang Province (2022E10022).

Disclosure

The authors state that they had no commercial or financial ties that could be perceived as a potential conflict of interest during the research.

References

1. Liu H, Huang Z, Chen H, et al., A potential strategy against clinical carbapenem-resistant Enterobacteriaceae: antimicrobial activity study of sweetener-decorated gold nanoparticles in vitro and in vivo. *J Nanobiotechnology*. 2023;21:409.
2. Jean SS, Harnod D, Hsueh PR. Global threat of carbapenem-resistant gram-negative bacteria. Front Cell Infect Microbiol. Available from: https://www.frontiersin.org/journals/cellular-and-infection-microbiology/articles/10.3389/fcimb.2022.823684/full. Accessed March 15, 2022.
3. Murray CJL, Ikuta KS, Sharara F. Antimicrobial Resistance Collaborators. Global burden of bacterial antimicrobial resistance in 2019: a systematic analysis. *Lancet*. 2022;399(10325):629–655. doi:10.1016/S0140-6736(21)02724-0
4. Rodríguez-Noriega E, Garza-González E, Bocanegra-Ibarias P, et al. A case–control study of infections caused by *klebsiella pneumoniae* producing New Delhi metallo-beta-lactamase-1: predictors and outcomes. *Front Cell Infect Microbiol*. 2022;12. 10.3389/fcimb.2022.867347
5. Wang L, Zheng W, Zhong L, et al. Phenylboronic acid-modified gold nanoclusters as a nanoantibiotic to treat vancomycin-resistant enterococcus faecalis-caused infections. *ACS Nano*. 2023;17(20):19685–19695. doi:10.1021/acsnano.3c02886
6. Wang Y, Malkmes MJ, Jiang C, et al., Antibacterial mechanism and transcriptome analysis of ultra-small gold nanoclusters as an alternative of harmful antibiotics against gram-negative bacteria. *J Hazard Mater*. 2021;416:126236.
7. Pelgrift RY, Friedman AJ. Nanotechnology as a therapeutic tool to combat microbial resistance. *Adv Drug Delivery Rev*. 2013;65(13):1803–1815.
8. Gupta A, Mumtaz S, Li CH, Hussain I, Rotello VM. Combatting antibiotic-resistant bacteria using nanomaterials. *Chem Soc Rev*. 2019;48(2):415–427. doi:10.1039/C7CS00748E
9. Chakraborty N, Jha D, Roy I, et al. Nanobiotics against antimicrobial resistance: harnessing the power of nanoscale materials and technologies. *J Nanobiotechnology*. 2022;20(1):375. doi:10.1186/s12951-022-01573-9
10. Prasad P, Gupta S. Nanobioconjugates: weapons against antibacterial resistance. *ACS Appl Bio Mater*. 2020;3(12):8271–8285. doi:10.1021/acsabm.0c01107
11. Szliszka E, Czuba ZP, Domino M, Mazur B, Zydowicz G, Krol W. Ethanolic extract of propolis (EEP) enhances the apoptosis- inducing potential of TRAIL in cancer cells. *Molecules*. 2009;14(2):738–754. doi:10.3390/molecules14020738
12. Tahlan S, Kumar S, Narasimhan B. Pharmacological significance of heterocyclic 1H-benzimidazole scaffolds: a review. *BMC Chem*. 2019;13(1):101. doi:10.1186/s13065-019-0625-4
13. Hayashi Y. Pot economy and one-pot synthesis. *Chem Sci*. 2016;7(2):866–880.
14. Andrews JM. Determination of minimum inhibitory concentrations. *J Antimicrob Chemother*. 2001;48(suppl_1):5–16. doi:10.1093/jac/48.suppl_1.5
15. Wang L, Zheng W, Li S, Zhong L, Jiang X. Aminophenol-decorated gold nanoparticles for curing bacterial infections. *Nano Lett*. 2022;22(9):3576–3582. doi:10.1021/acs.nanolett.1c04968
16. Huang Z, Liu H, Zhang X, et al. Ceftazidime-decorated gold nanoparticles: a promising strategy against clinical ceftazidime-avibactam-resistant enterobacteriaceae with different resistance mechanisms. *Antimicrob Agents Chemother*. 2023;67(7):e00262–23. doi:10.1128/aac.00262-23

17. Liu X, Xiong Y, Shi Y, et al. In vitro activities of licochalcone A against planktonic cells and biofilm of enterococcus faecalis. *Front Microbiol*. 2022;13:970901. doi:10.3389/fmicb.2022.970901
18. Huang Z, Zhang X, Yao Z, et al. Thymol-decorated gold nanoparticles for curing clinical infections caused by bacteria resistant to last-resort antibiotics. *mSphere*. 2023;8(3):e0054922. doi:10.1128/msphere.00549-22
19. Dobrovolskaia MA, Clogston JD, Neun BW, Hall JB, Patri AK, McNeil SE. Method for analysis of nanoparticle hemolytic properties in vitro. *Nano Lett*. 2008;8(8):2180–2187. doi:10.1021/nl0805615
20. Hu P, Chen H, Zhao D, et al. Azomycin orchestrate colistin-resistant enterobacter cloacae complex's colistin resistance reversal in vitro and in vivo. *ACS Infect Dis*. 2024;10(2):662–675. doi:10.1021/acsinfecdis.3c00526
21. Bailly A-L, Correard F, Popov A, et al. In vivo evaluation of safety, biodistribution and pharmacokinetics of laser-synthesized gold nanoparticles. *Sci Rep*. 2019;9(1):12890. doi:10.1038/s41598-019-48748-3
22. Helander IM, Mattila-Sandholm T. Fluorometric assessment of gram-negative bacterial permeabilization. *J Appl Microbiol*. 2000;88(2):213–219. doi:10.1046/j.1365-2672.2000.00971.x
23. Wang Y, Kong J, Zhang X, et al. Plumbagin resurrect colistin susceptible against colistin-resistant pseudomonas aeruginosa in vitro and in vivo. *Front Microbiol*. 2022;13. Available from: https://www.frontiersin.org/journals/microbiology/articles/10.3389/fmicb.2022.1020652/full. Accessed February 14, 2025.
24. Ehtt J, Dc R, N C, Dz M, W I. Antimicrobial and anti-biofilm peptide octominin for controlling multidrug-resistant acinetobacter baumannii. *Int J mol Sci*. 2021;22(10). Available from: https://pubmed.ncbi.nlm.nih.gov/34069596/. Accessed February 14, 2025.
25. Xiao FX, Zeng Z, Liu B. Bridging the gap: electron relay and plasmonic sensitization of metal nanocrystals for metal clusters. *J Am Chem Soc*. 2015;137(33):10735–10744. doi:10.1021/jacs.5b06323
26. Hoebe KHN, Monshouwer M, Witkamp RF, Fink-Gremmels J, van Miert ASJPAM. Cocultures of porcine hepatocytes and kupffer cells as an improved in vitro model for the study of hepatotoxic compounds. *Vet Q*. 2000;22(1):21–25. doi:10.1080/01652176.2000.9695018
27. Choudhury D, Ahmed Z. Drug-associated renal dysfunction and injury. *Nat Rev Nephrol*. 2006;2(2):80–91. doi:10.1038/ncpneph0076
28. Daems N, Verlinden B, Van Hoecke K, et al. In vivo pharmacokinetics, biodistribution and toxicity of antibody-conjugated gold nanoparticles in healthy mice. *J Biomed Nanotechnol*. 2020;16(6):985–996. doi:10.1166/jbn.2020.2928
29. Yang H, Du L, Tian X, et al. Effects of nanoparticle size and gestational age on maternal biodistribution and toxicity of gold nanoparticles in pregnant mice. *Toxicol Lett*. 2014;230(1):10–18.
30. Slavin YN, Asnis J, Häfeli UO, Bach H. Metal nanoparticles: understanding the mechanisms behind antibacterial activity. *J Nanobiotechnol*. 2017;15(1):65. doi:10.1186/s12951-017-0308-z
31. Chen H, Hu P, Liu H, et al. Combining with domiphen bromide restores colistin efficacy against colistin-resistant gram-negative bacteria in vitro and in vivo. *Int J Antimicrob Agents*. 2024;63(2):107066.
32. Xie W, Zhang S, Pan F, et al. Nanomaterial-based ROS-mediated strategies for combating bacteria and biofilms. *J Mater Res*. 2021;36(4):822–845. doi:10.1557/s43578-021-00134-4
33. Soria-Segarra C, Soria-Segarra C, Molina-Matute M, et al. Molecular epidemiology of carbapenem-resistant gram-negative bacilli in ecuador. *BMC Infect Dis*. 2024;24(1):378. doi:10.1186/s12879-024-09248-6
34. Aiesh BM, Maali Y, Qandeel F, et al. Epidemiology and clinical characteristics of patients with carbapenem-resistant enterobacterales infections: experience from a large tertiary care center in a developing country. *BMC Infect Dis*. 2023;23(1):644. doi:10.1186/s12879-023-08643-9
35. Verma A, Stellacci F. Effect of surface properties on nanoparticle–cell interactions. *Small*. 2010;6(1):12–21. doi:10.1002/smll.200901158
36. Li K, Hein S, Zou W, Klug G. The glutathione-glutaredoxin system in rhodobacter capsulatus: part of a complex regulatory network controlling defense against oxidative stress. *J Bacteriol*. 2004;186(20):6800–6808. doi:10.1128/JB.186.20.6800-6808.2004
37. Rosenberg G, Yehezkel D, Hoffman D, et al. Host succinate is an activation signal for salmonella virulence during intracellular infection. *Science*. 2021;371(6527):400–405. doi:10.1126/science.aba8026
38. Noster J, Persicke M, Chao T-C, et al. Impact of ROS-induced damage of TCA cycle enzymes on metabolism and virulence of salmonella enterica serovar typhimurium. *Front Microbiol*. 2019;10:10. doi:10.3389/fmicb.2019.00010